Published in final edited form as:
Cancer Invest. 2009 May ; 27(4): 435–442. doi:10.1080/07357900802491477.

Osteoblastic and Osteolytic Human Osteosarcomas can be Studied with a new Xenograft Mouse Model Producing Spontaneous Metastases

Jun Yuan[*,1,2], **Christian Ossendorf**[*,2], **Jan P. Szatkowski**[3], **James T. Bronk**[3], **Avudaiappan Maran**[3], **Michael Yaszemski**[3], **Mark E. Bolander**[3], **Gobinda Sarkar**[3,4], and **Bruno Fuchs**[2]

[1]Children's Cancer Institute of Australia for Medical Research, Randwick, Australia [2]Department of Orthopaedics, Balgrist University Hospital, University of Zurich, Zurich, Switzerland [3]Department of Orthopaedics, Mayo Clinic, Rochester, MN [4]Department of Experimental Pathology, Mayo Clinic, Rochester, MN

Abstract

There is no animal model that reflects the histological and radiographical heterogeneity of osteosarcoma. We assessed seven osteosarcoma cell lines for their potential to develop orthotopic tumors and lung metastasis in SCID mice. Whereas radiologically, 143B developed osteolytic tumors, SaOS-LM7 developed osteoblastic primary tumors. The mineralization status was confirmed by assessing the alkaline phosphatase activity and the microarray expression profile. We herein report a xenograft orthotopic osteosarcoma mouse model to assess osteoblastic and osteolytic lesions, which may contribute in the search for new diagnostic and therapeutic approaches.

Keywords

Osteosarcoma; Animal Model; Xenograft; Orthotopic; Lung metastasis

Introduction

Human osteosarcoma (OS) is the most common primary bone cancer predominantly affecting children and adolescents and one of the most frequent causes of cancer-related deaths in childhood.[1,2] Approximately 25% of OS metastasize, typically to the lung. Despite effective surgical removal of the primary tumor and aggressive chemotherapy, pulmonary metastasis is associated with poor prognosis.[3,4,5]

The pathogenesis of OS metastasis remains poorly understood at both the cellular and molecular levels. Therefore, accurate testing of therapeutic strategies to improve disease-free survival of OS patients is difficult with the present animal models. OS is heterogeneous histologically and radiographically. It has been hypothesized that the heterogeneity of tumors may contribute to the lack of effectiveness of drug therapies against metastasis,[6] which also influences prognosis. Animal models of OS metastasis reflecting this heterogeneity may

Corresponding author: Bruno Fuchs, MD, PhD, Department of Orthopaedics, Balgrist University Hospital, University of Zurich, Zurich, Forchstrasse 340, Switzerland. Phone: +41 44 386 1661; Fax: +41 44 386 1669; E-mail: Bruno.Fuchs@balgrist.ch.
*These two authors contributed equally to the work.

Declaration of interest: the authors report no conflict of interest. The authors alone are responsible for the content and writing of the paper.

contribute to successful evaluation of new drugs and therapeutic concepts to fight OS. There are murine, syngeneic OS models using cell lines such as Dunn, LM8, K12, K7M2 or UMR106-01[6,7,8,9,10] and xenograft models using human OS cell lines U2OS, TE85 and derivatives thereof (HOS, MNNG, KRIB, 143B, and SaOS-2).[11,12,8,13,14,15]

A prerequisite for an adequate OS model is the mimicking of the genetics, biology and etiology of the human disease including response to therapeutic agents; allowance for the analysis of tumor progression and spread within 1–2 months; cellular expression of markers that are biological signatures of OS such as osteocalcin (OCN), alkaline phosphatase (AP), pro-1-collagen (COL), matrix-Gla-protein (MGP), osteopontin (OPN); production of osteoid matrix, and pulmonary metastasis.[16,17,18] With classification primarily based on histology, more than twelve different histological subtypes of OS were described.[19,20,21]

From these, teleangiectatic OS was associated with a high rate of pathologic fractures, although patients with this OS subtype had no worse prognosis than patients with other high grade subtypes.[22] Except for histology, important diagnostic criteria of OS are location and radiological appearance. Here, OS can be either osteolytic, osteoblastic or mixed osteolytic-osteoblastic. However, the significance of this observation is poorly understood. We may speculate that this heterogeneity may contribute to confounding factors on the side of patients. To better understand this mixed radiological appearance, we need to be able to use appropriate animal models reflecting this heterogeneity. Therefore we have developed an orthotopic xenograft OS mouse model to answer the following questions: Is there tumor formation after local (orthotopic) injection of the OS cell lines investigated here and do they develop lung metastasis? Is there a correlation of radiological appearance of the orthotopic tumor and molecular and biological aspects of OS?

Materials and methods

Cell lines and tissue culture

Human OS cell lines G292, MG-63, TE85, U2OS, SaOS-2 and 143B were purchased from the American Type Culture Collection (ATCC, Rockville, MD, USA). SaOS-LM7 cells were kindly provided by Dr. E. Kleinerman (M.D. Anderson Cancer Center, TX, USA). Cells were cultured in 75cm^2 tissue culture flasks in Dulbecco's Modified Eagle Medium (DMEM), supplemented with 10% heat-inactivated fetal calf serum (FCS), 2 mM L-glutamine, 100U/ml penicillin, and 50 U/ml streptomycin at 37° C in an atmosphere of 5% CO_2.

Animals and animal care

All procedures and protocols were approved by the IACUC of the Mayo Clinic (Rochester, MN, USA). NOD/SCID mice (*prkdc*^{scid}, The Jackson Laboratory, Bar Harbor, ME, USA) were purchased at 4 weeks of age and kept in a sterile environment in plastic cages bedded with sterilized soft wood granulate and given at least one week to adapt to their new environment prior to surgery. The mice were fed an autoclaved cereal-based diet *ad libitum* along with pasteurized and acidified tap water. Five animals per cage were housed, with 12 h light-dark cycle, in a central animal care facility of our institution. All manipulations on the animals were performed under sterile conditions and all animals were subjected to regular health checks. Mice were anesthetized with buprenorphine (2mg/kg, s.c.), ketamine (90 mg/kg) and xyline (10 mg/kg, i.m.) before manipulations.

Intratibial (orthotopic) implantation of single cell suspensions

After harvesting, cells were brought to a final concentration of 1×10^6 cells per ml in phenol-free HBSS and kept at 4° C. The cells were assessed for viability using Trypan blue staining. Experiments were continued only if cell viability was greater than 90%. Preliminary injection

studies yielded that the injection of 100 μl established the best results. Hence a volume of 100 μl (1×10^6 cells) cell suspension was used for both i.v. and orthotopic injections. Animals were anesthetized and the right leg disinfected with 70% ethanol. Cells were aspirated into a 1 ml tuberculin syringe fitted with a 27 G needle. The needle was inserted through the cortex of the anterior tuberosity of the tibia with a rotating "drill-like" movement to avoid cortical fracture (Figure 1). Once the bone was traversed, the needle was inserted further to fracture the posterior cortex of the tibia as described elsewhere.[23] 100 μl of cell suspension was injected while slowly moving back the needle. Tibial tumor growth and size of the respective extremity were assessed 3–4 days after inoculation of tumor cells. Radiograms were taken at 2, 4, and 6 weeks post-injection using a Picker-Sureview mammography device (Picker International, Highland Heights, OH, USA) and a Kodak Min-B screen cassette and corresponding film (Eastman Kodak, Rochester, NY, USA), with a molybdenum anode and filter under the following conditions: focus 0.2 mm, 24 kw exposure 12 mAs, distance 60 cm, magnification factor 1.5.

Assessment of local tumor growth

Tibial tumor growth was observed twice a week beginning 1 week after inoculation of tumor cells. The volume of the tumor was calculated as described previously[24,25] by using the following equation: volume = (L + W) (L) (W) (0.2618). The value assigned as width (W) was the average of the anterior–posterior and medial–lateral planes at the proximal tibia at the level of the knee joint. The value assigned as length (L) was the distance from the most distal extent of the calf musculature or distal tumor margin to the knee joint or proximal tumor margin. The tumor doubling time during the log phase of growth was calculated using the following equation: t = (log2)/slope of the log of tumor volume vs. days.

Histopathological assessment of primary tumors and pulmonary metastases

The mice were euthanized by CO_2 inhalation. Primary tumors from the tibia were excised and the tumor size was measured. Lungs, kidneys, livers, and spleens were dissected, fixed with 10% formalin and embedded in paraffin. Bone was decalcified prior to embedding by 5% formic acid overnight. Formation of metastases in the lung was detected by gross observation and histopathological assessment. Briefly, visible tumor nodules (macrometastases) were counted and measured with the aid of a dissecting microscope. The embedded specimens were serially cut in a longitudinal fashion (5 μm thick sections), and every 10^{th} section was HE stained. Five sections of each tissue were examined. For assessment of pulmonary metastases, each stained section was examined microscopically under low power (12.5 ×) to visualize approximately 50% of the lung section per microscopic field. The total number of metastases per lung section was counted and the average was calculated.

Leg amputation (hip disarticulation)

To investigate if pulmonary metastasis resulted from orthotopic primary tumor growth mice were orthotopically inoculated with SaOS-LM7 and 143B cells and early amputation was performed by hip disarticulation 30 min after injection of the cells, to avoid tumor cells that underwent intravasation to get into the venous system by pressure resulting from orthotopic injection. All animals were anesthetized thirty minutes after tumor cell implantation. Surgery was performed under sterile conditions. An oval skin incision was made around the right hip joint. The neurovascular bundle in the groin was identified; the vessels were coagulated with bipolar diathermia and divided. The leg was dissected from the hip joint. Then, the muscles were re-sutured over the acetabulum, and the skin was closed. After surgery, the mice were kept on warm plates until they recovered from anesthesia. An additional dose of 2mg/kg of buprenorphine was given subcutaneously 12 h after surgery. Both groups (amputated and control) were autopsied at 5 weeks (143B) and 10 weeks (SaOS-LM7) after inoculation.

AP activity and mineralization assay

Cellular differentiation was evaluated using a specific AP activity detection kit (Chemicon, Billerica, MA, USA). In brief, confluent cells in 6-well plates were rinsed three times with ice-cold PBS, scraped in distilled water, and sonicated. AP activity of the cell lysates was determined colorimetrically using phenyl phosphate (PNP) as a substrate. Protein concentrations of cell lysates were measured by the Micro BCA protein assay (Pierce, Rockford, IL, USA) following the manufacturer's instructions. The reaction was stopped with 0.1 M NaOH, and the absorbance was read at 405 nm. Each value was normalized with the value in protein content. The mineralization of cells was determined in 6 well plates using von Kossa staining.[26,27] Results were expressed as percentage of the control cell line SaOS-2.

After confluent cells were grown in DMEM supplemented with 10% FBS, 1% penicillin/streptomycin, 50 ug/ml ascorbic acid, and 10 mM glycerophosphate for 4 weeks, they were fixed with 95% ethanol and stained with $AgNO_3$ to detect phosphate deposits in bone tumors.

Microarray analysis of 143B and SaOS-LM7 cells

All microarray experiments including were done at the Mayo Microarray Core Facility. Biotinylated cRNAs were synthesized from 10 μg of total RNA, labeled, fragmented and hybridized to an Affymetrix U133A Plus 2.0 Gene Chip according to the manufacturer's protocol (Affymetrix, Santa Clara, CA, USA). Preprocessing of the Affymetrix arrays was carried out using Microarray Suite 5.0. Gene expression intensity for each array was scaled to an average arbitrary value of 1500 intensity units to allow comparisons across all arrays. Duplicate microarray experiments were carried out for each cell line (143B and SaOS-LM7). Genes that were significantly overexpressed ($p<0.05$) were ranked according to their expression levels and compared between SaOS-LM7 and 143B, and vice versa. Descriptive statistics and Student's t-test were done using Excel (Microsoft, Redmond, WN, USA).

Results

Orthotopic tumor formation after intratibial OS cell line injection

To assess their tumorigenic potential, 7 established OS tumor cell lines (G292, MG-63, TE85, U2OS, SaOS-2, 143B, and SaOS-LM7) were injected into the proximal tibia of NOD/SCID mice (Figure 1A). G292 and TE85 developed neither orthotopic tumors nor lung metastasis. U2OS formed lung metastasis in 1/7 mice only. In contrast, injection of MG-63 and SaOS-2 cell lines showed histological evidence of local tumor formation in 2/7 and 4/7 mice (Table 1) in the proximal tibia 112 days after inoculation. The tumors were of osteoblastic phenotype and exhibited new bone formation (Figure 1C). All mice (8/8) injected with 143B cells developed tumors and osteolytic lesions were seen five weeks post-injection (Figure 1B). Primary tumors resulting from 143B cells exhibited radiographic and histological features characteristic of human primary OS, including central osteolytic, highly undifferentiated cell type, and marked bone destruction observed increased osteoclasts along the destroyed bone in the 143B generated tumors (Figure 1D). After injection of SaOS-LM7 cells, all animals (n=10) developed primary tumors. Eight weeks after inoculation, these animals showed radiographic evidence of tumor formation. New bone formation in the primary SaOS-LM7 tumors was seen in the periosteum and in the soft tissues, while the proximal ends of the tibia remained intact (Figure 1E).

Metastatic tumor formation after orthotopic injection of OS cell lines

No macro-metastases to extrapulmonary sites, including liver, spleen, kidney, and lymph nodes were detected. No lung metastasis was found in mice injected with MG-63 and SaOS-2 cells, even though there was some local tumor development in the tibia (Table 1). Metastatic lung

nodules were absent in all animals that underwent leg amputation, while all control animals developed marked pulmonary lesions. Intratibial injection of 143B cells resulted in spontaneous lung metastasis in 7/8 mice and in 5/10 of mice injected with SaOS-LM7 cells (Table 1, Figure 3A, B).

Comparison of AP activity and bone mineralization potential of 143B and SaOS-LM7 cells

Bone formation capacity of different OS cell lines was evaluated *in vitro* using AP activity and mineralization assays as markers of mature osteoblastic differentiation. SaOS-LM7 cells expressed high levels of AP (297 ± 17%) compared with their parental cell lines (Figure 4). After four weeks of culture in a medium supplemented with ascorbic acid and glycerol phosphate, mineralized nodules were absent in the 143B cell culture (Figure 5A). SaOS-2 and SaOS-LM7 cells developed large areas of mineralization, with microscopically prominent mineral nodules (143 ± 25 calcified nodules per well, Figure 5 B and C). These results suggest that SaOS-LM7 cells possess a higher capacity for bone formation than 143B cells, which is consistent with the radiological osteoblastic and osteolytic phenotypes of OS in our animal model.

Microarray evaluation of SaOS-LM7 and 143B cells

We speculated that osteoblastic and osteolytic tumor formation by SaOS-LM7 and 143B cells may be due to their intrinsic osteoblastic and osteolytic characteristics. Thus, we subjected these two cell lines to microarray analysis and compared differentially expressed genes between these two cell lines. No gene appeared to be highly over-expressed in 143B cells compared to SaOS-LM7 cells and only a few genes, like COL13A1, MMP1, SERPIND1 and NMES1 showed two-fold over-expression. In contrast, many genes appear to be highly over-expressed in SaOS-LM7 cells compared to expression in 143B cells. Genes encoding for collagen-transcripts like COL3A1, COL1A1, COL8A1, PCOLCE (procollagen C-endopeptidase enhancer), or COL5A1 were abundantly expressed by the SaOS-LM7 cells. COL3A1 was 674 fold stronger expressed in SaOS-LM7 than in 143B, COL1A1 60-fold, COL8A1 9-fold, PCOLCE 8-fold and COLC5A1 6-fold. A 10-fold over-expression of the core binding factor 1(cbfa 1) in SaOS-LM7 compared to 143B cells confirms that the radiological picture of osteoblastic and osteolytic patterns are also reflected at the molecular level, because cbfa1 is an essential gene for osteoblastic maturation and subsequent bone formation.

Discussion

In the present study, we have developed a xenograft OS mouse model by investigating tumor formation after orthotopic injection of 7 established human OS cell lines and correlated radiological appearances of the respective orthotopic tumors with molecular and biological aspects of OS in highly overexpressed genes. Tumors generated by orthotopic injection of 143B and SaOS-LM7 cells in NOD/SCID mice produced lung metastasis at high frequency after a short period of time. The mouse model presented here reflects an osteoblastic and osteolytic phenotype of human OS, which also may lead to a deeper understanding of cellular, molecular and physiological characteristics and help exploring novel drug-candidates against OS.

Concerning tumor formation after orthotopic injection of SaOS-2 and 143B as well as expression of AP, we could confirm previously reported findings.[28] COL1A1 was abundantly expressed in the SaOS-LM7 compared to 143B in the present study. However, high COL1A1 expression has been described for G292 and SaOS-2, but not for 143B cells.[28]

The first report of an OS xenograft system with occurrence of spontaneous metastasis of a human sarcoma was by Berlin et al. in 1993 using a v-Ki-*ras* transformed HOS cell line (KRIB

or 143B).[11] With numbers of 1000–20000 cells per mouse orthotopically injected but a different volume and without penetrating the cortex of the tibial bone compared to our study, local tumor growth and lung metastasis were assessed after 8 weeks time. Both G292 and TE85 cell lines were able to form orthotopic tumors anchored to adjacent periostea without showing differences between the cell lines.[29] In the present study, primary orthotopic tumor formation resulted after injection of TE85 cells and not after injection of G292 cells. This might be due to different inoculation techniques, as apart from orthotopic injections, a surgical exposure technique was used. However, it is not clear whether the inbred strain (NOD/SCID mice (*prkdc*^{scid})) that has been used in our study was also used in this investigation.

Orthotopically injected 143B cells developed both primary tumors and lung metastasis in our study confirming previously published results.24 Also in line with previously published findings,[24] we could not see lung metastasis after orthotopic injection of TE85 cells. 143B formed local tumors and lung metastasis with high efficiency while TE85 cells were not able to form any tumors neither locally nor metastatic. Overlays of fluorescence and X-ray image demonstrated destructive processes of the proximal tibia with associated pathologic fractures. [24] In another study, both SaOS-2 and 143B formed primary tumors in all eight injected mice, but only SaOS-2 and not 143B formed metastasis.[28] These two studies differed greatly in the amount of cells used: 20000 versus 1×10^6 per mouse. However, from studies investigating tibial tumor take rate and development of lung metastasis after injection of KRIB cells it became clear that as less as 1000 tumor cells are sufficient to induce orthotopic tibial tumors and lung metastasis.[11] The same authors presented data that the majority of pulmonary lesions occurring subsequent to orthotopic inoculation of KRIB cells originate from cells resident for at least 24 h in the injected tibia and that induced tibial tumors must grow locally for at least 14 days before metastasis seeding to the lungs can occur.[4]

Slow cancer progression and low frequency of metastasis limit the application of the SaOS-2 model, despite its high frequency of lung metastasis after tail vein injection.[13,30] In contrast, SaOS-LM6 cells were described to colonize the lung with superior ability.[13] Here, we could show tumor formation in local and metastatic sites (proximal tibia and lung) with relatively fast progression after intratibial implantation of SaOS-LM7 cells. Interestingly, inoculation of SaOS-LM7 resulted in 100% of primary osteoblastic tumor development and also produced pulmonary metastasis in 50% of animals. The abundant expression of the collagen genes and an approximately ten-fold over-expression of cbfa1 in SaOS-LM7 cells compared to 143B cells as demonstrated by our microarray experiments may provide a testable rationale that tumors produced by SaOS-LM7 cells are osteoblastic. Assessment of the interactions between tumor and the host microenvironment is the strength of syngeneic models. However, these models are often characterized by tumor growth in heterotopic sites. They are therefore unsuitable for mimicking radiological features of human OS like osteolytic or osteoblastic lesions and for that reason could not be employed in the present study. Moreover, they cannot be used for assessment of chemotherapeutic agents to find new therapies to fight OS. In addition to subcutaneous OS models which were largely inconsistent in value and size of tumor formations[28] probably due to or depending on the injection technique, there have also been intramuscular approaches proposed recently.[23,31] Compared to these, the advantage of orthotopic OS models is that they allow for studying orthotopic primary tumor formation as well as the metastatic progression of OS reconstituting the entire metastatic process.[28] In contrast, models employing intravenous injection of OS tumor cells ensure reliable reproduction of pulmonary metastasis and steps later in the metastatic cascade at the cost of omitting the early steps.

There is a significant amount of radiographic heterogeneity in OS such as osteoblastic and osteolytic lesions which needs to be experimentally addressed for successful development of novel therapeutic regimens. Whether the etiologies underlying predominantly osteoblastic or

predominantly osteolytic tumors are the same and how they differ in progression of the disease, in their metastatic potential and their response to chemotherapeutic drugs will have to be investigated in future studies.

Several reports explain osteolytic destruction patterns of human OS to be most likely caused by osteoclasts and tumor cells.[32,33] In our study, we observed increased osteoclasts along the destroyed bone in the 143B generated tumors. An increase in osteoclast activity is most likely caused by production of local factors such as PTHrP, transforming growth factor beta, IL-1, IL-6, IL-11, and TNF-alpha that stimulate osteoclastic resorption of bone.[34,35] Another possibility is that tumor cells themselves destroy bone directly. When compared with other OS cells (including SaOS-LM7), high expression of MMP1 and other proteases from our microarray data in 143B cells provides a potential mechanism underlying production of osteolytic lesions by 143B cells.

In conclusion, the xenograft animal model presented here replicates the heterogeneity of OS to improve the understanding of the underlying pathobiology. It is the first OS animal model that specifically emphasizes the osteoblastic and osteolytic radiographic appearance of human OS, thereby complementing and extending the value of the existing models. Our xenograft model further aims to explore mechanisms underlying human OS progression and metastasis and thereby may contribute to the evaluation of novel therapeutics and future improvements of existing chemotherapeutic regimens against OS.

Acknowledgement

We thank Ming Ruan, Phimolsarnti Rapin, MD and Beata Bode, MD for their technical assistance. This work was supported by the NIH grant AR47974.

References

1. Gatta G, Capocaccia R, Coleman MP, Ries LA, Berrino F. Childhood cancer survival in Europe and the United States. Cancer 2002;95:1767–1772. [PubMed: 12365026]
2. Howe HL, Wu X, Ries LA, Cokkinides V, Ahmed F, Jemal A, Miller A, Williams M, Ward E, Wingo PA. Ramirez A, Edwards BK. Annual report to the nation on the status of cancer, 1975–2003, featuring cancer among U.S. Hispanic/Latino populations. Cancer 2006;107:1711–1742. [PubMed: 16958083]
3. Link MP. Adjuvant therapy in the treatment of osteosarcoma. Important Adv Oncol 1986:193–207. [PubMed: 3330533]
4. Link MP, Goorin AM, Miser AW, Green AA, Pratt CB, Belasco JB, Pritchard J, Malpas JS, Baker AR, Kirkpatrick JA, et al. The effect of adjuvant chemotherapy on relapse-free survival in patients with osteosarcoma of the extremity. N Engl J Med 1986;314:1600–1606. [PubMed: 3520317]
5. Shanley DJ, Mulligan ME. Osteosarcoma with isolated metastases to the pleura. Pediatr Radiol 1991;21:226. [PubMed: 2047165]
6. Sandberg AA, Bridge JA. Techniques in cancer cytogenetics: an overview and update. Cancer Invest 1992;10:163–172. [PubMed: 1551026]
7. Asai T, Ueda T, Itoh K, Yoshioka K, Aoki Y, Mori S, Yoshikawa H. Establishment and characterization of a murine osteosarcoma cell line (LM8) with high metastatic potential to the lung. Int J Cancer 1998;76:418–422. [PubMed: 9579581]
8. Dunn TB, Andervont HB. Histology of some neoplasms and non-neoplastic lesions found in wild mice maintained under laboratory conditions. J Natl Cancer Inst 1963;31:873–901. [PubMed: 14173606]
9. Khanna C, Prehn J, Yeung C, Caylor J, Tsokos M, Helman L. An orthotopic model of murine osteosarcoma with clonally related variants differing in pulmonary metastatic potential. Clin Exp Metastasis 2000;18:261–271. [PubMed: 11315100]
10. Martin TJ, Ingleton PM, Underwood JC, Michelangeli VP, Hunt NH, Melick RA. Parathyroid hormone-responsive adenylate cyclase in induced transplantable osteogenic rat sarcoma. Nature 1976;260:436–438. [PubMed: 1062678]

11. Berlin O, Samid D, Donthineni-Rao R, Akeson W, Amiel D, Woods VL Jr. Development of a novel spontaneous metastasis model of human osteosarcoma transplanted orthotopically into bone of athymic mice. Cancer Res 1993;53:4890–4895. [PubMed: 8402677]
12. Chen X, Li Y, Xiong K, Aizicovici S, Xie Y, Zhu Q, Sturtz F, Shulok J, Snodgrass R, Wagner TE, Platika D. Cancer gene therapy by direct tumor injections of a nonviral T7 vector encoding a thymidine kinase gene. Hum Gene Ther 1998;9:729–736. [PubMed: 9551620]
13. Jia SF, Worth LL, Kleinerman ES. A nude mouse model of human osteosarcoma lung metastases for evaluating new therapeutic strategies. Clin Exp Metastasis 1999;17:501–506. [PubMed: 10763916]
14. Jones PA, Rhim JS, Isaacs H Jr. McAllister RM. The relationship between tumorigenicity, growth in agar and fibrinolytic activity in a line of human osteosarcoma cells. Int J Cancer 1975;16:616–621. [PubMed: 1080752]
15. Manara MC, Baldini N, Serra M, Lollini PZ, DeGiovanni C, Vaccari M, Argnani A, Benini S, Maurici D, Picci P, Scotlandi K. Reversal of malignant phenotype in human osteosarcoma cells transduced with the alkaline phosphatase gene. Bone 2000;26:215–220. [PubMed: 10709992]
16. Dass CR, Ek ET, Choong PF. Human xenograft osteosarcoma models with spontaneous metastasis in mice: clinical relevance and applicability for drug testing. J Cancer Res Clin Oncol 2007;133:193–198. [PubMed: 17031670]
17. Ek ET, Dass CR, Choong PF. Commonly used mouse models of osteosarcoma. Crit Rev Oncol Hematol 2006;60:1–8. [PubMed: 16837208]
18. Zhou H, Choong P, McCarthy R, Chou ST, Martin TJ, Ng KW. In situ hybridization to show sequential expression of osteoblast gene markers during bone formation in vivo. J Bone Miner Res 1994;9:1489–1499. [PubMed: 7817834]
19. Ilaslan H, Sundaram M, Unni KK, Shives TC. Primary vertebral osteosarcoma: imaging findings. Radiology 2004;230:697–702. [PubMed: 14749514]
20. Inwards CY, Unni KK. Classification and grading of bone sarcomas. Hematol Oncol Clin North Am 1995;9:545–569. [PubMed: 7649942]
21. Tebbi CK, Gaeta J. Osteosarcoma. Pediatr Ann 1988;17:285–300. [PubMed: 3290815]
22. Tsai YC, Mendoza A, Mariano JM, Zhou M, Kostova Z, Chen B, Veenstra T, Hewitt SM, Helman LJ, Khanna C, Weissman AM. The ubiquitin ligase gp78 promotes sarcoma metastasis by targeting KAI1 for degradation. Nat Med 2007;13:1504–1509. [PubMed: 18037895]
23. Khanna C, Wan X, Bose S, Cassaday R, Olomu O, Mendoza A, Yeung C, Gorlick R, Hewitt SM, Helman LJ. The membrane-cytoskeleton linker ezrin is necessary for osteosarcoma metastasis. Nat Med 2004;10:182–186. [PubMed: 14704791]
24. Luu HH, Kang Q, Park JK, Si W, Luo Q, Jiang W, Yin H, Montag AG, Simon MA, Peabody TD, Haydon RC, Rinker-Schaeffer CW, He TC. An orthotopic model of human osteosarcoma growth and spontaneous pulmonary metastasis. Clin Exp Metastasis 2005;22:319–329. [PubMed: 16170668]
25. Luu HH, Zagaja GP, Dubauskas Z, Chen SL, Smith RC, Watabe K, Ichikawa Y, Ichikawa T, Davis EM, Le Beau MM, Rinker-Schaeffer CW. Identification of a novel metastasis-suppressor region on human chromosome 12. Cancer Res 1998;58:3561–3565. [PubMed: 9721861]
26. Sowa H, Kaji H, Yamaguchi T, Sugimoto T, Chihara K. Activations of ERK1/2 and JNK by transforming growth factor beta negatively regulate Smad3-induced alkaline phosphatase activity and mineralization in mouse osteoblastic cells. J Biol Chem 2002;277:36024–36031. [PubMed: 12130649]
27. Sowa H, Kaji H, Yamaguchi T, Sugimoto T, Chihara K. Smad3 promotes alkaline phosphatase activity and mineralization of osteoblastic MC3T3-E1 cells. J Bone Miner Res 2002;17:1190–1199. [PubMed: 12096832]
28. Dass CR, Ek ET, Contreras KG, Choong PF. A novel orthotopic murine model provides insights into cellular and molecular characteristics contributing to human osteosarcoma. Clin Exp Metastasis 2006;23:367–380. [PubMed: 17187230]
29. Yang SY, Yu H, Krygier JE, Wooley PH, Mott MP. High VEGF with rapid growth and early metastasis in a mouse osteosarcoma model. Sarcoma 2007;2007:95628. [PubMed: 18274612]
30. Jia SF, Zhou RR, Kleinerman ES. Nude mouse lung metastases models of osteosarcoma and Ewing's sarcoma for evaluating new therapeutic strategies. Methods Mol Med 2003;74:495–505. [PubMed: 12415717]

31. Tsai YC, Mendoza A, Mariano JM, Zhou M, Kostova Z, Chen Z, Veenstra T, Hewitt SM, Helman LJ, Khanna C, Weissman AM. The ubiquitin ligase gp78 promotes sarcoma metastasis by targeting KAI1 for degradation. Nat Med 2007;13:1504–1509. [PubMed: 18037895]

32. Chirgwin JM, Guise TA. Molecular mechanisms of tumor-bone interactions in osteolytic metastases. Crit Rev Eukaryot Gene Expr 2000;10:159–178. [PubMed: 11186331]

33. Giuliani N, Pedrazzoni M, Passeri G, Girasole G. Bisphosphonates inhibit IL-6 production by human osteoblast-like cells. Scand J Rheumatol 1998;27:38–41. [PubMed: 9506876]

34. Guise TA, Yoneda T, Yates AJ, Mundy GR. The combined effect of tumor-produced parathyroid hormone-related protein and transforming growth factor-alpha enhance hypercalcemia in vivo and bone resorption in vitro. J Clin Endocrinol Metab 1993;77:40–45. [PubMed: 8325957]

35. Suarez-Cuervo C, Harris KW, Kallman L, Väänänen HK, Selander KS. Tumor necrosis factor-alpha induces interleukin-6 production via extracellular-regulated kinase 1 activation in breast cancer cells. Breast Cancer Res Treat 2003;80:71–78. [PubMed: 12889600]

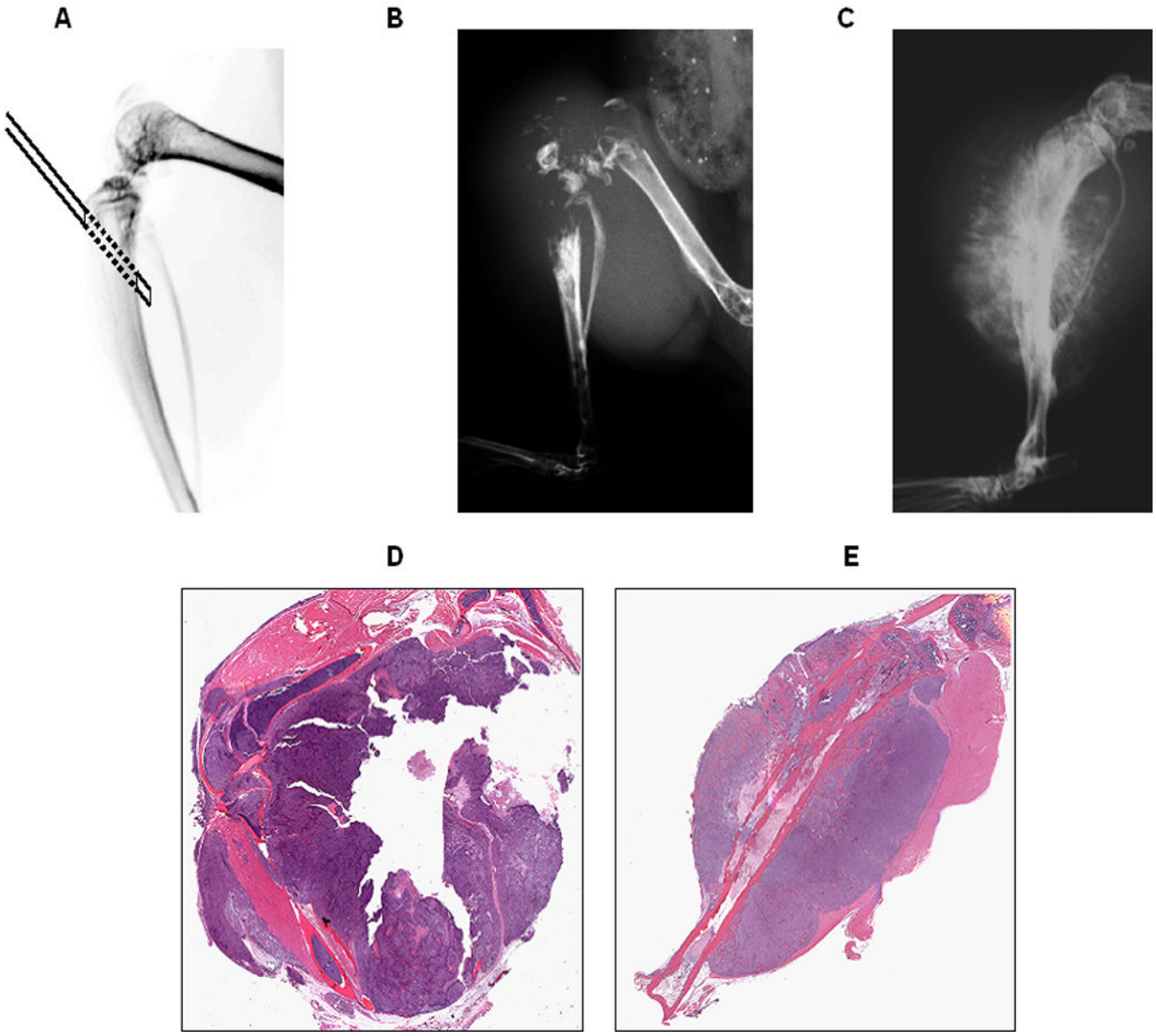

Figure 1.
Cell implantation technique and orthotopic tumor formation: 1×10^6 cells in 100 μl HBSS were injected orthotopically into the tibia and the surrounding soft tissue with a 27G needle penetrating the posterior wall of the tibia (A). Representative radiographs of the extremities of mice 5 weeks after injection of 143B cells (B) and 10 weeks after injection of SaOS-LM7 cells are shown (C). Primary tumors from the tibia and the surrounding soft tissue were paraffin-embedded, sectioned, and H&E stained 5 weeks after injection of 143B cells (D) and 10 weeks after injection of SaOS-LM7 cells (E).

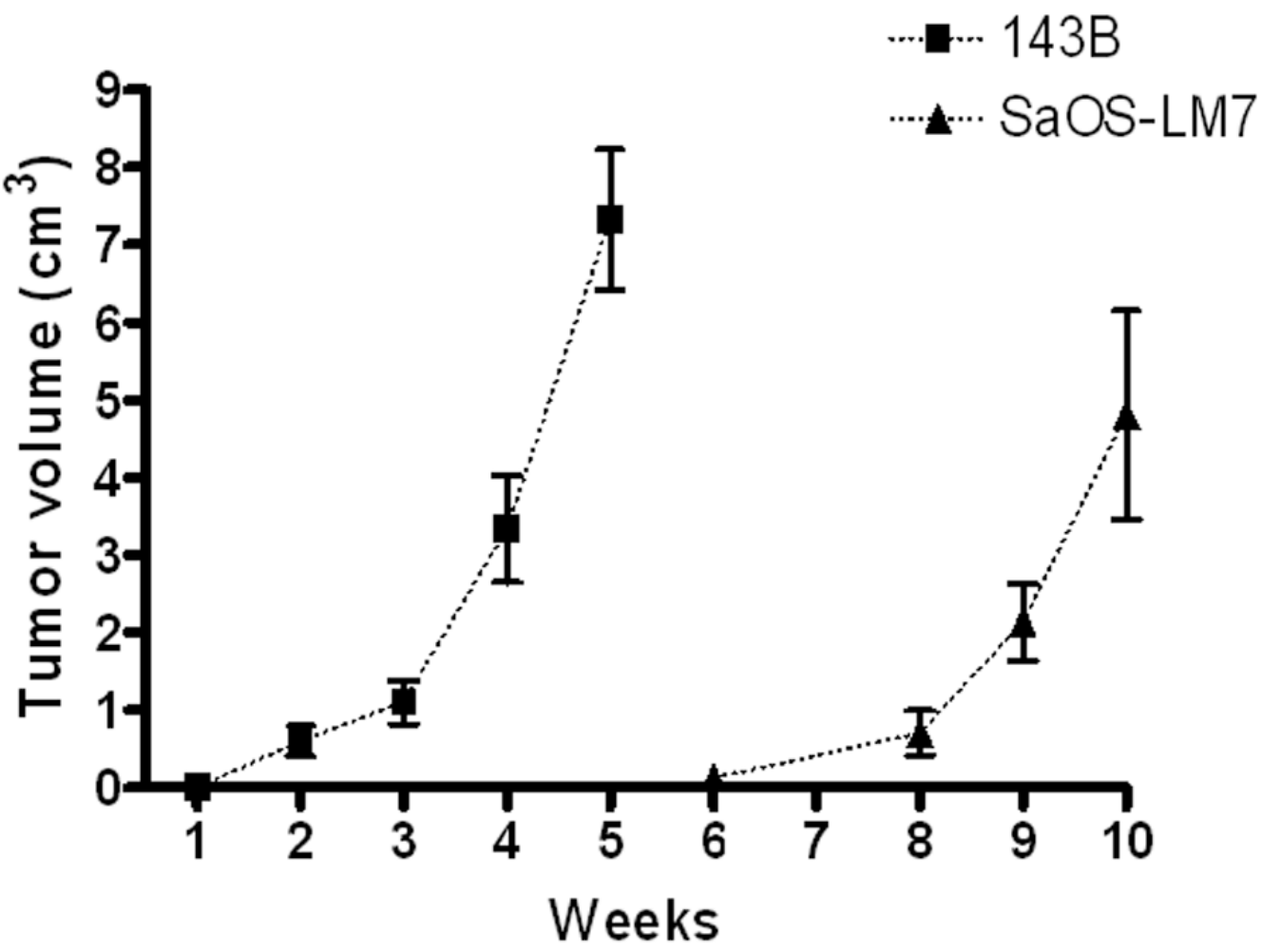

Figure 2.
Comparison of tibial tumor growth in SaOS-LM8 and 143B cells. Tumor volume was measured in animals after injection with 143B cells and SaOS-LM7 cells for indicated period.

A

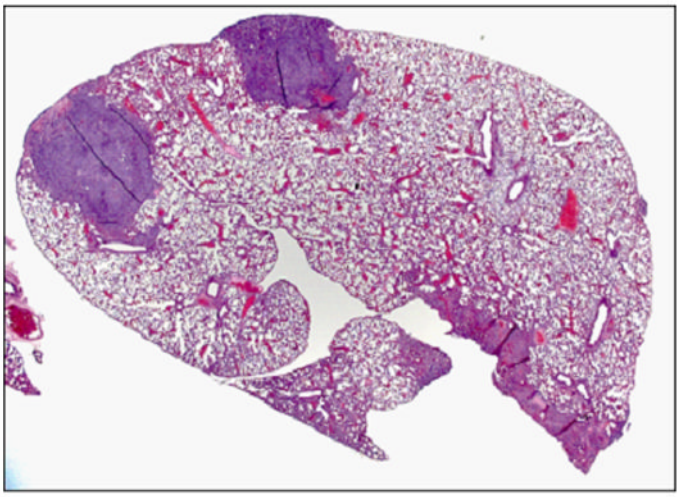

B

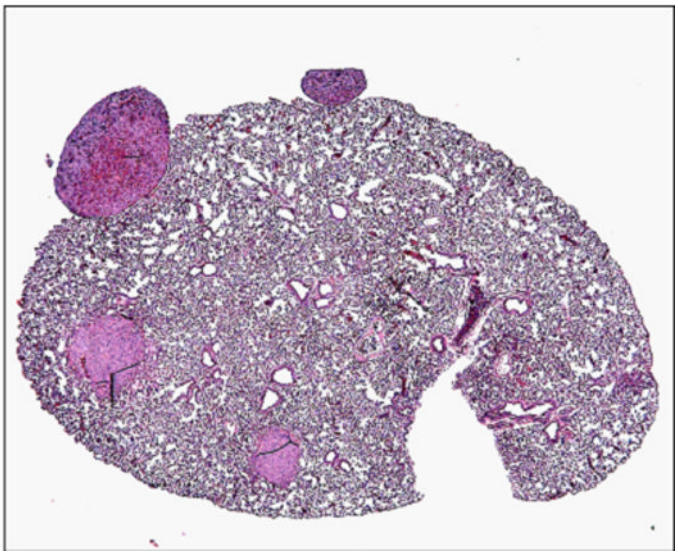

Figure 3.
Lung tissues containing metastasis (insert) were paraffin-embedded, sectioned, and H&E stained 5 weeks after intra-osseous injection of 143B cells (A) and 10 weeks after injection of SaOS-LM7 cells (B).

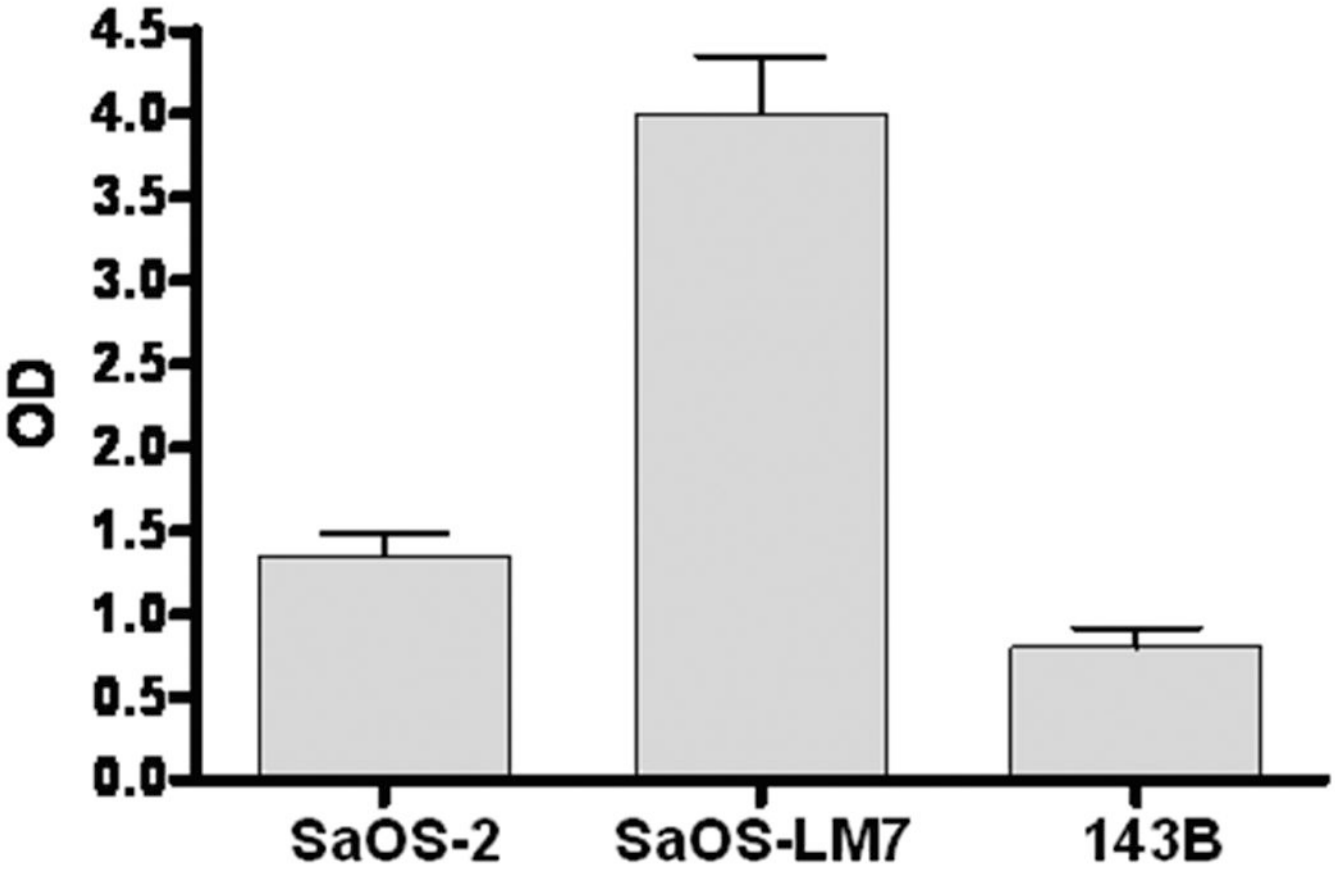

Figure 4.
Alkaline phosphatase activity levels in various tumor cell lines: levels of alkaline phosphatase activity were determined in SaOS-2, SaOS-LM7 and 143B cells and expressed percentage of the control cell line SaOS-2 (n=6).

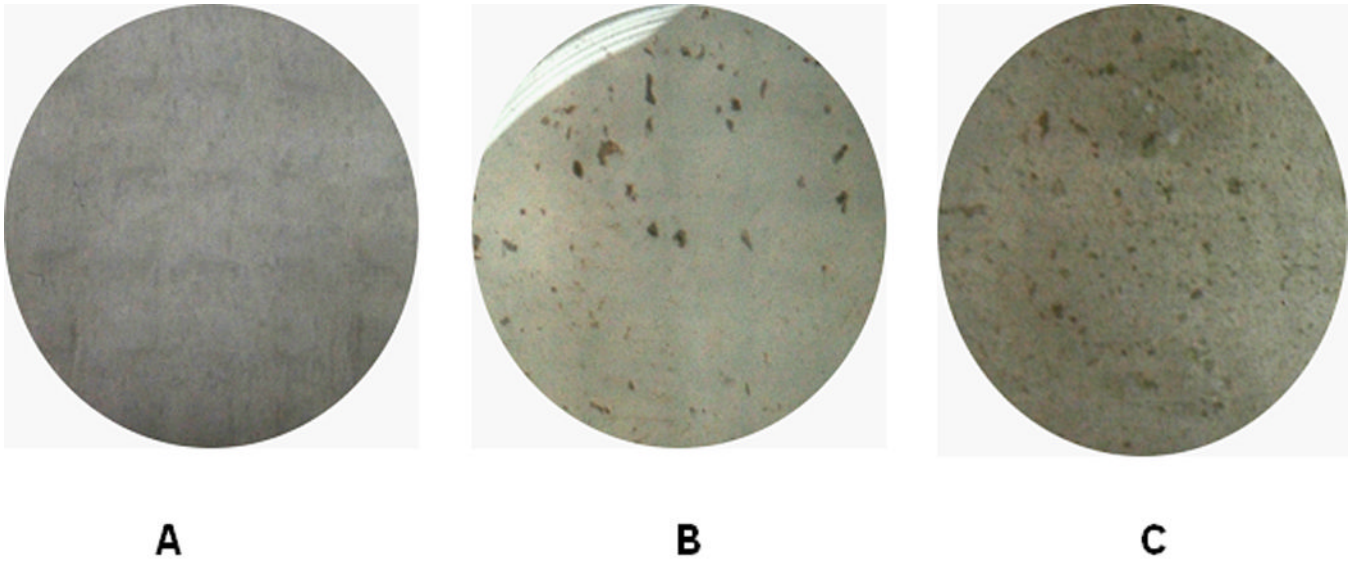

Figure 5.
After four weeks of culture, 143B (A), SaOS-2 (B), and SaOS-LM7 (C) cells formed mineralization nodules with increasing frequency.

Table 1

Local tumor formation and metastasis after orthotopic injection into the tibia

Injected Cells	Doubling time *in vivo* (hours)	Number of mice in each group (n)	Time of Sacrifice (days)	Number of mice with tumors in tibia	Number of mice with metastatic tumors	Location of metastasis
143B	12	8	35	8/8 (100 %)	7/8 (88 %)	Lung
MG-63	28	7	112	2/7 (29 %)	0/7 (0 %)	(-)
SaOS-2	16	7	112	4/7 (57 %)	0/7 (0 %)	(-)
SaOS-LM7	22	10	70	10/10 (100 %)	5/10 (50 %)	Lung